Supporting Information

Achieving High Efficiency in Solution-Processed Perovskite Solar Cells using C_{60}/C_{70} Mixed Fullerenes

Hao-Sheng Lin[1], Il Jeon[1], Rong Xiang[1], Seungju Seo[1], Jin-Wook Lee[2], Chao Li[2], Amrita Pal[3], Sergei Manzhos[3], Mark S.Goorsky[2], Yang Yang[2], Shigeo Maruyama[1], and Yutaka Matsuo[1,4]**

[1]Department of Mechanical Engineering, The University of Tokyo, 7-3-1 Hongo, Bunkyo-ku, Tokyo 113-8656, Japan

[2]Department of Materials Science and Engineering, University of California, Los Angeles, Los Angeles, CA 90095, USA

[3]Department of Mechanical Engineering, National University of Singapore, Block EA #07-08, 9 Engineering Drive 1, Singapore 117576, Singapore

[4]Hefei National Laboratory for Physical Sciences at the Microscale, University of Science and Technology of China, Hefei, Anhui 230026, China

*corresponding to il.jeon@spc.oxon.org (I.J) and matsuo@photon.t.u-tokyo.ac.jp (Y.M)

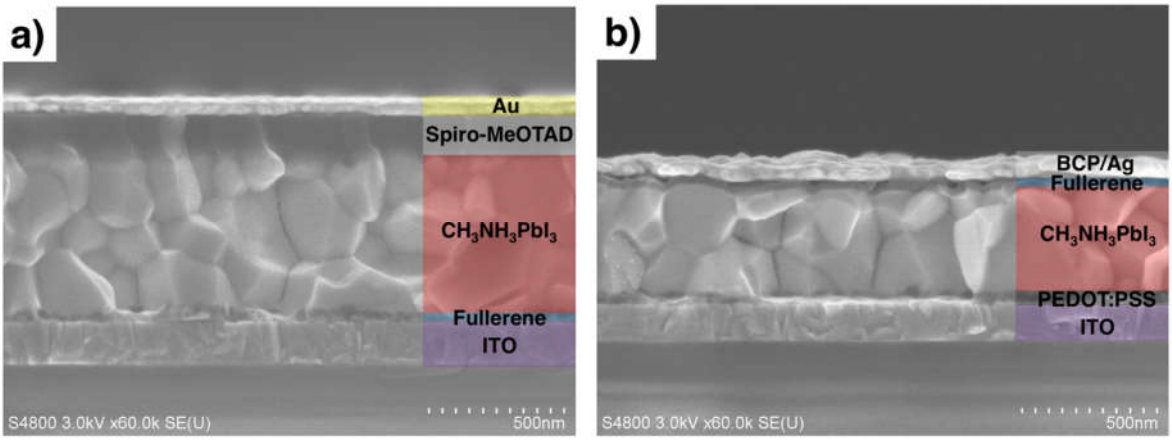

Figure S1. Cross-sectional SEM images of a) normal-type PSCs and b) inverted-type PSCs.

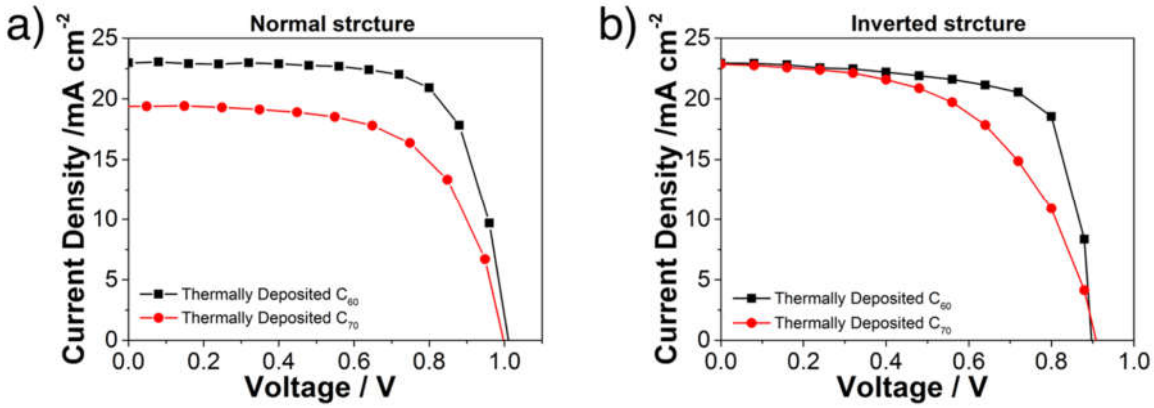

Figure S2. *J–V* curves of the thermally deposited C_{60}- (black squares and line) and C_{70}- (red circles and line) based PSC for a) the normal-type structure and b) the inverted-type structure.

a) Frontier orbital comparison of single molecules at the DFT level: [6-31+G(d,p)]

The calculations were performed in Gaussian 09[S1] with the 6-31+g(d,p) basis, in vacuum.

HOMO-LUMO distributions:

C_{60} HOMO LUMO

C_{70} HOMO LUMO

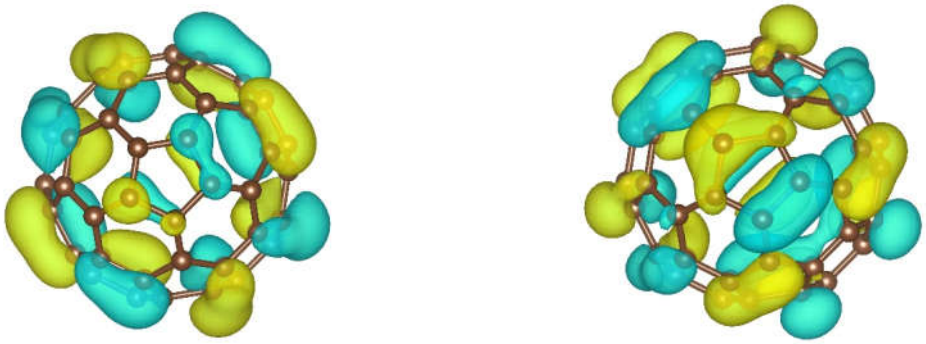

The HOMO-LUMO values are as below:

With the B3LYP[S2] functional (quantitative)

C_{60}: HOMO: -6.40 eV C_{70}: HOMO: -6.33 eV

LUMO: -3.68 eV LUMO: -3.67 eV

With the PBE[S3] functional (for comparison to DFTB)

C_{60}: HOMO: -5.86 eV C_{70}: HOMO: -5.86 eV

LUMO: -4.21 eV LUMO: -4.16 eV

b) Energy level comparison of single molecules at the DFTB level:

The calculations were performed in DFTB+[S4] using the 3ob-3-1[S5,S6] parameter set

The HOMO-LUMO distributions:

C_{60} HOMO LUMO

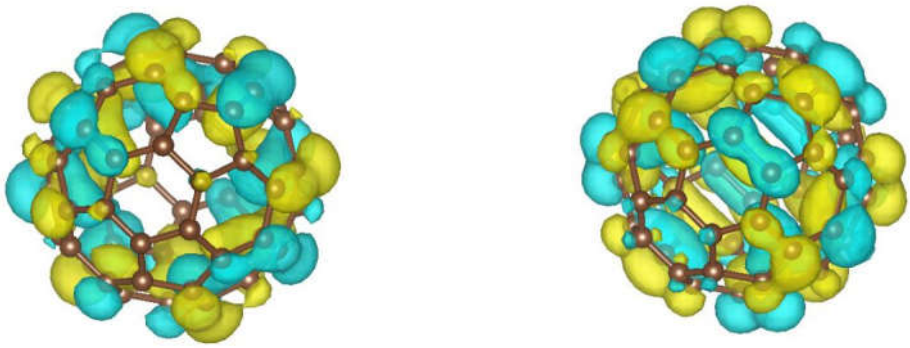

C_{70} HOMO LUMO

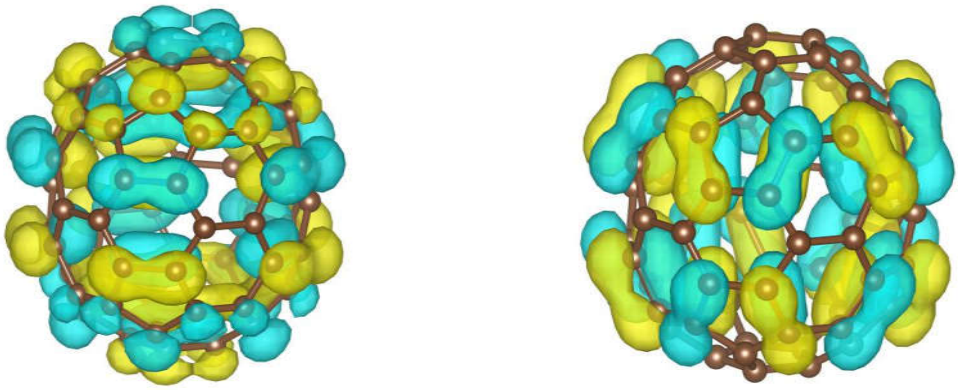

The HOMO-LUMO values are as below:

C_{60}: HOMO: -5.67 eV C_{70}: HOMO: -5.60 eV

LUMO: -3.88 eV LUMO: -3.97 eV

Figure S3. Frontier orbital calculations of C_{60} and C_{70} a) at the DFT level, and b) at the DFTB level. [S1–S6]

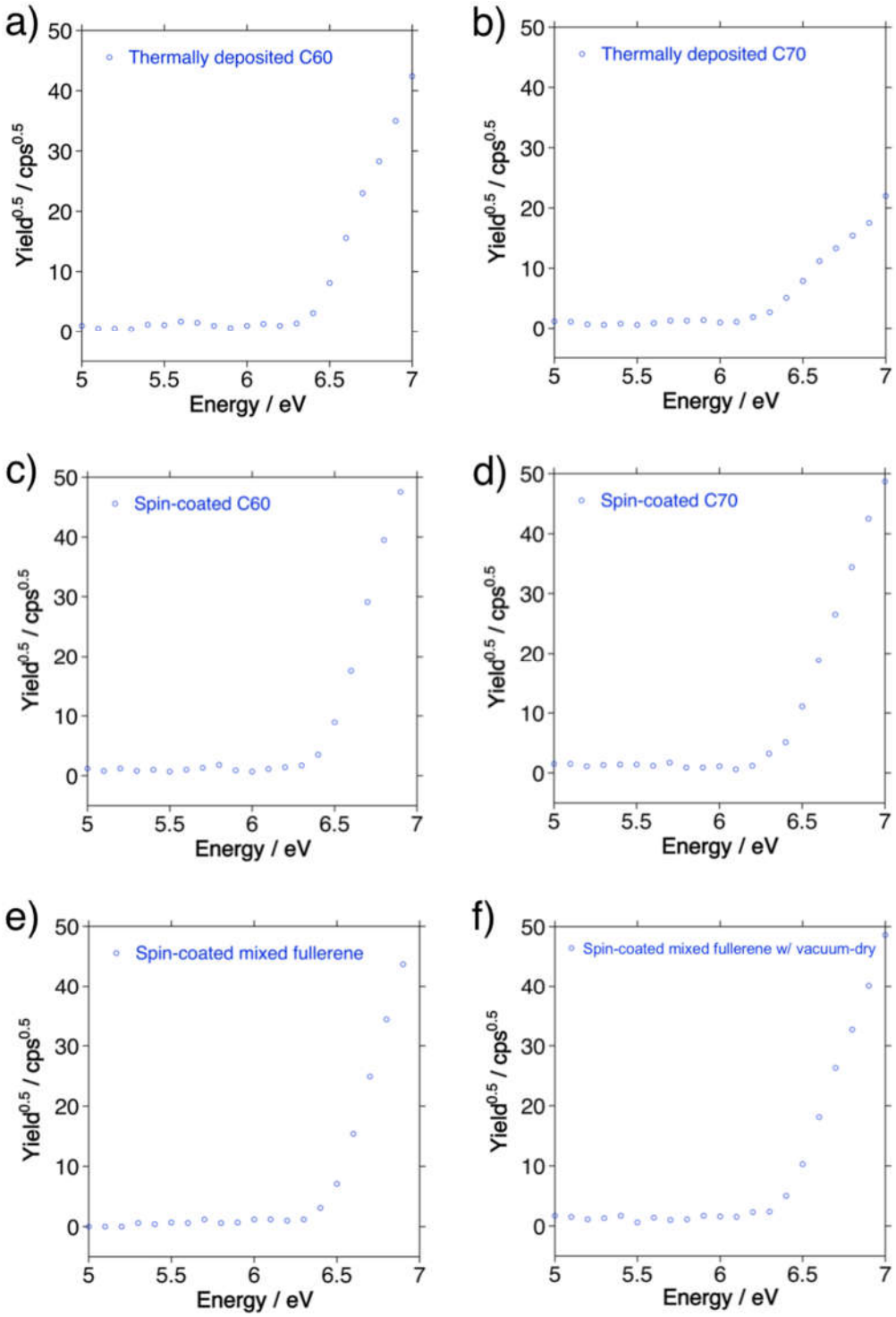

Figure S4. PYS spectra of a) thermally deposited C_{60}, b) thermally deposited C_{70}, c) spin-coated C_{60}, d) spin-coated C_{70}, e) spin-coated C_{60}/C_{70} (9:1), and f) vacuum-dried spin-coated C_{60}/C_{70} (9:1).

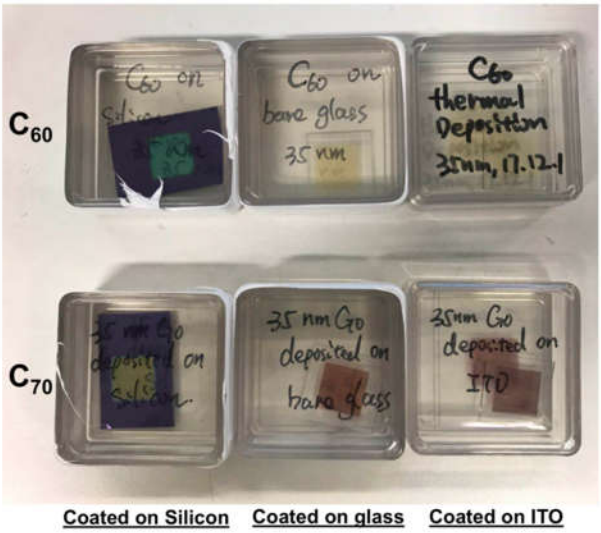

Figure S5. Various C_{60} and C_{70} films on glass and silicon substrates. The difference in transparency between C_{60} and C_{70} of the same thickness is visible even for the naked eye.

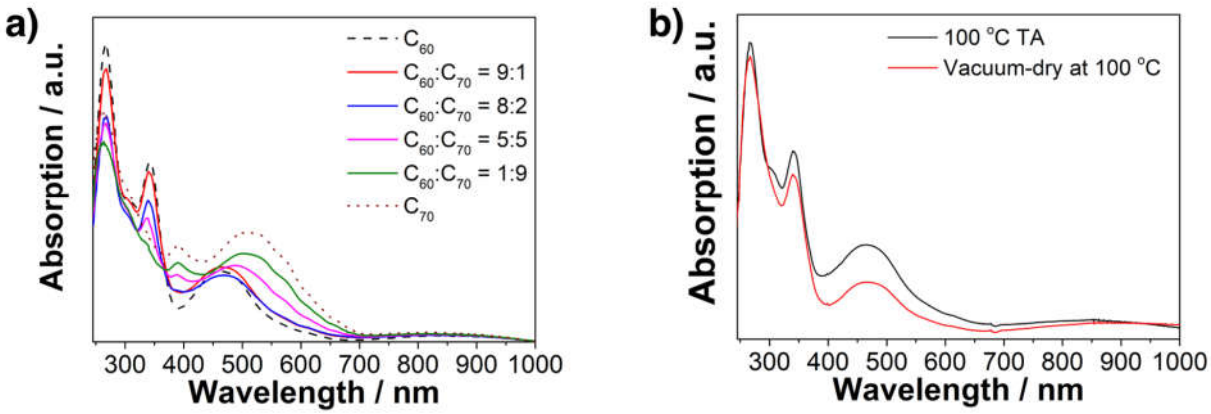

Figure S6. a) UV-vis absorption of spin-coated fullerene films with different C_{60} to C_{70} ratios. b) UV-vis absorption spectroscopy of thermally deposited C_{60} and C_{70}.

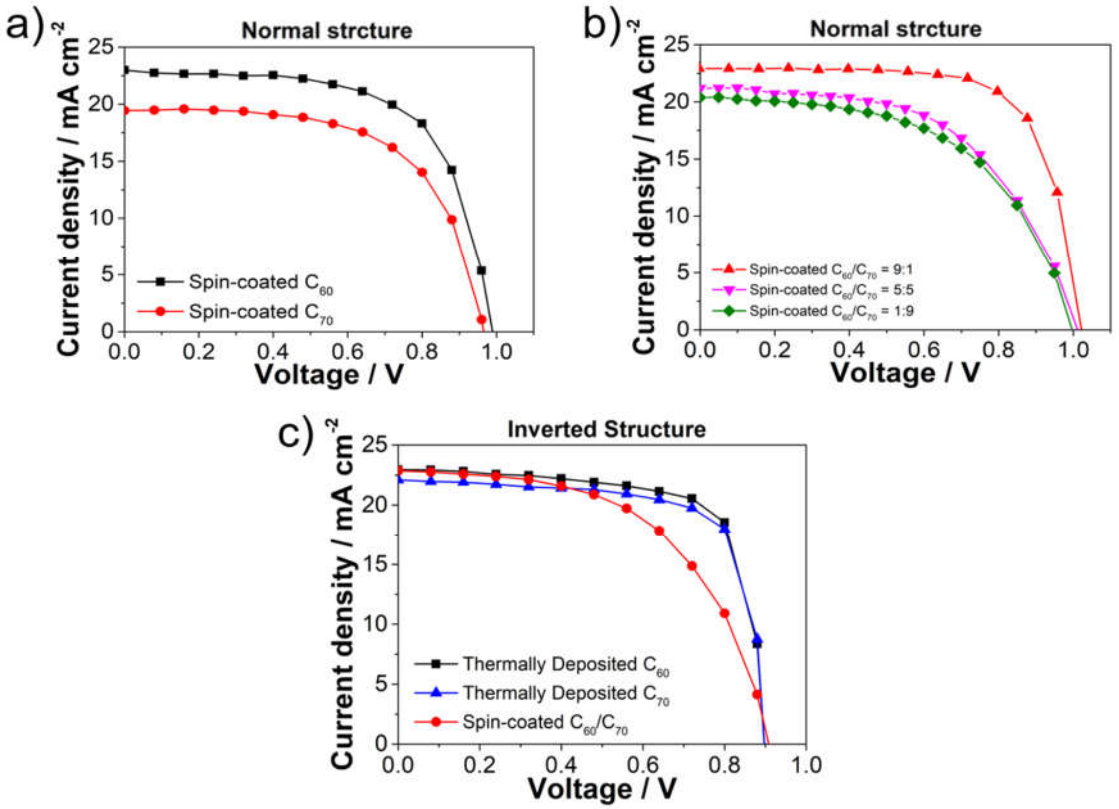

Figure S7. *J–V* curves of a) the normal-type PSCs using spin-coated C_{60}- (black) and C_{70}- (red); the normal-type PSCs using b) mixed fullerenes with different C_{60} to C_{70} ratios; c) the inverted-type PSCs using thermally deposited C_{60}- (black) and C_{70}- (red), and mixed fullerenes (blue).

Table S1. Photovoltaic parameters of the inverted-type PSCs using thermally deposited C_{60}, thermally deposited C_{70}, and spin-coated mix-fullerene as the ETLs under one sun (AM 1.5 G, 100 mW cm^{-2}).

Fullerene	J_{SC} [mA cm^{-2}]	V_{OC} [V]	FF	R_S [Ω cm^2]	R_{SH} [Ω cm^2]	PCE_{Best}	$PCE_{Average}$	Hysteresis Index
C_{60}	22.9	0.90	0.77	9	$1.1x10^4$	15.8%	15.3% ±0.4	0.01
C_{60}/C_{70}=9:1	22.1	0.90	0.76	10	$1.0x10^4$	15.2%	15.0% ±0.5	0.01
C_{70}	22.9	0.91	0.55	27	$7.2x10^3$	11.4%	11.3% ±0.3	0.02

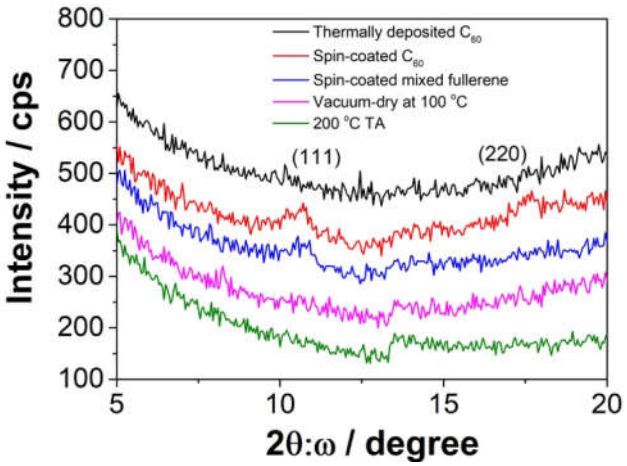

Figure S8. GIXRD scan of the thermally deposited C_{60} film (black), the spin-coated C_{60} film (red), the spin-coated mixed fullerene film (blue), the vacuum-dried mixed fullerene film (purple), and 200 °C TA-treated mixed fullerene film.

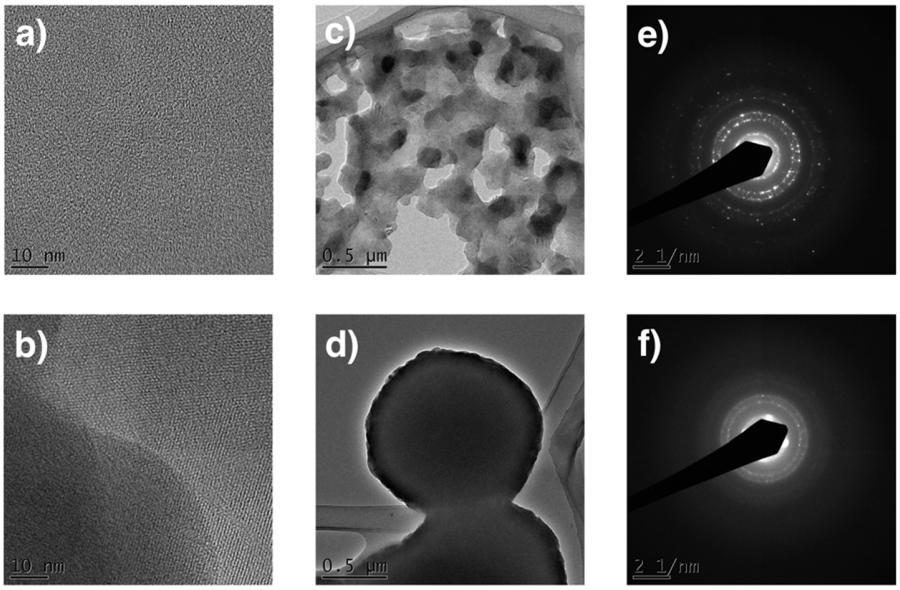

Figure S9. Supplementary TEM images of a) a thermally deposited C_{60} film, b) a boundary of crystal domains in a spin-coated C_{60} film, c) many crystal domains in a spin-coated C_{60} film, d) one large uniform domain in a mixed fullerene film, and supplementary SAED of e) a spin-coated C_{60} film and f) a mixed fullerene film.

Comparison of solids at the DFTB level (dispersion correction with the Grimme scheme):[S7]

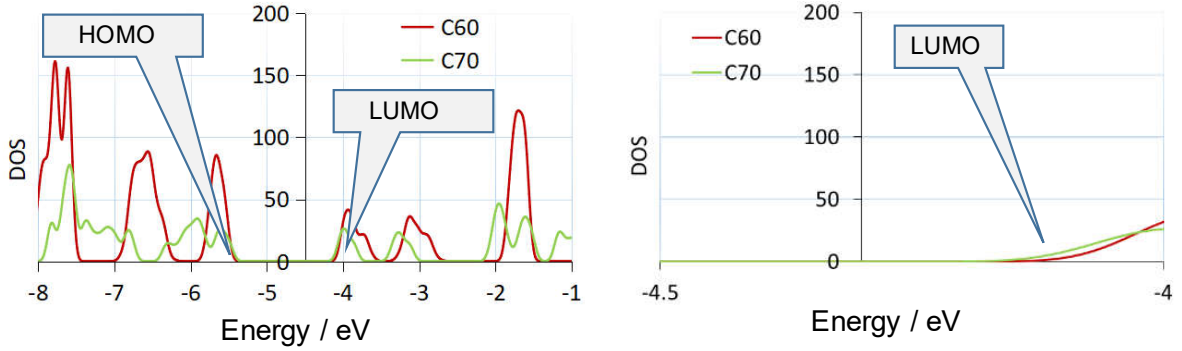

a) Density of states (DOS) of C_{60} and C_{70} crystals (left) with the LUMO magnified (right), showing the C_{60} and C_{70} LUMO position separately.

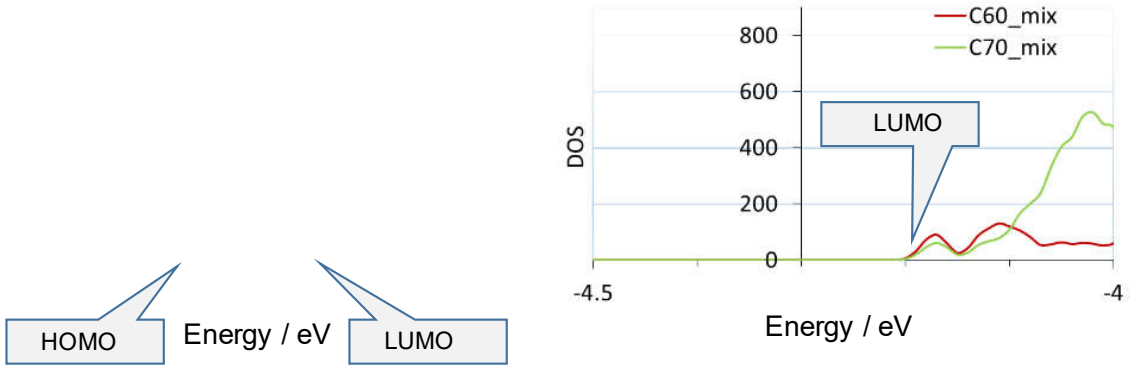

b) DOS of C_{60} and C_{70} parts in the mixed C_{60}/C_{70} structure.

Figure S10. Densities of states of a) C_{60} and C_{70}, and b) mixed fullerene (C_{60}:C_{70} 29:3) in solid state at the DFTB level. [S7]

Effect of surfaces on the band structure of C_{60} and C_{70}:

111 surface of C_{60} in fcc structure:

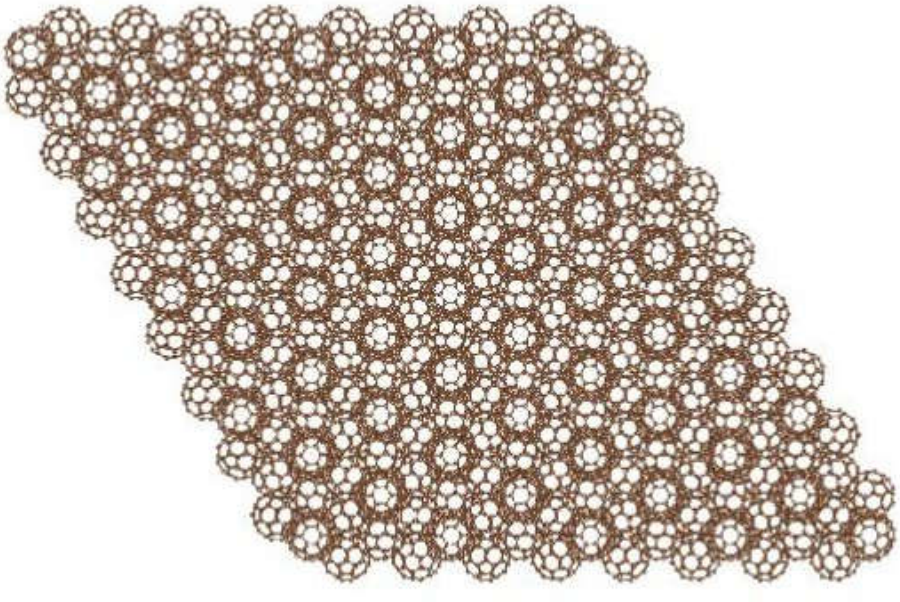

DOS of C_{60} and 111 surface of C_{60}:

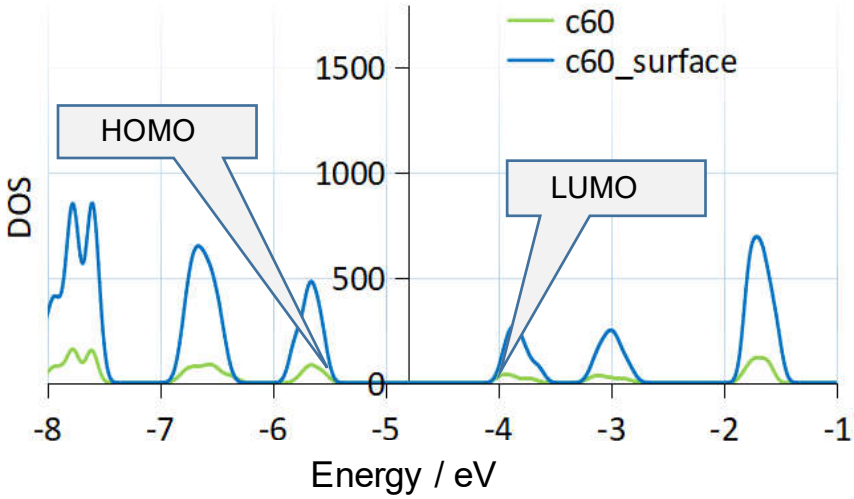

001 surface of C_{70} in hcp structure:
Similar to C_{60}, we cut the 001 surface of C_{70} hcp crystal.

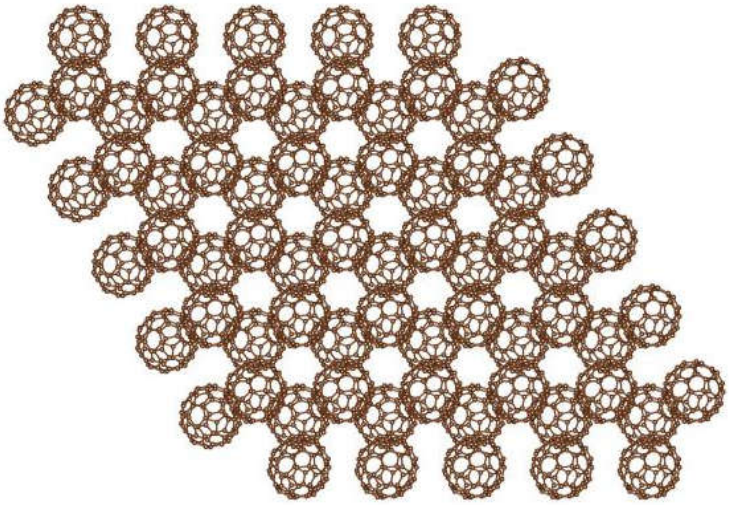

DOS of C_{70} and 001 surface of C_{70}:

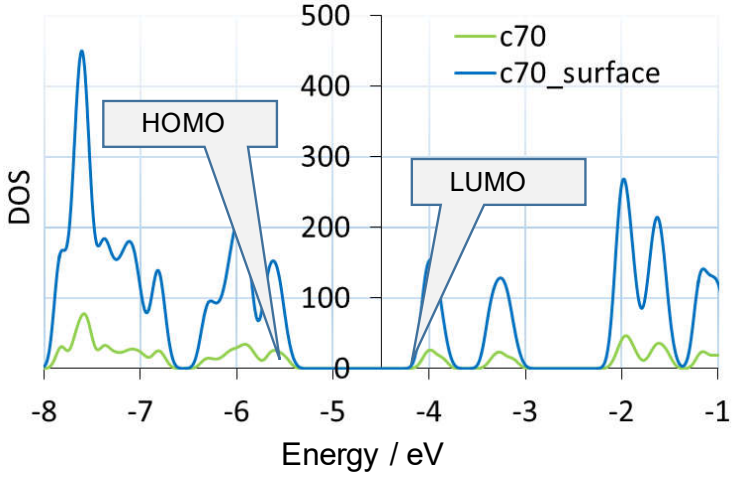

The lowest energy surfaces of both the C_{60} and C_{70} crystal behave similar with the bulk.

Figure S11. Computational energy level calculations of C_{60}, C_{70} , and mixed fullerene in which crystallinity and surface have been taken into account in solid at DFTB level.

Convex hull: The formation energies of C_{60}, and C_{70} and the mixed fullerene.

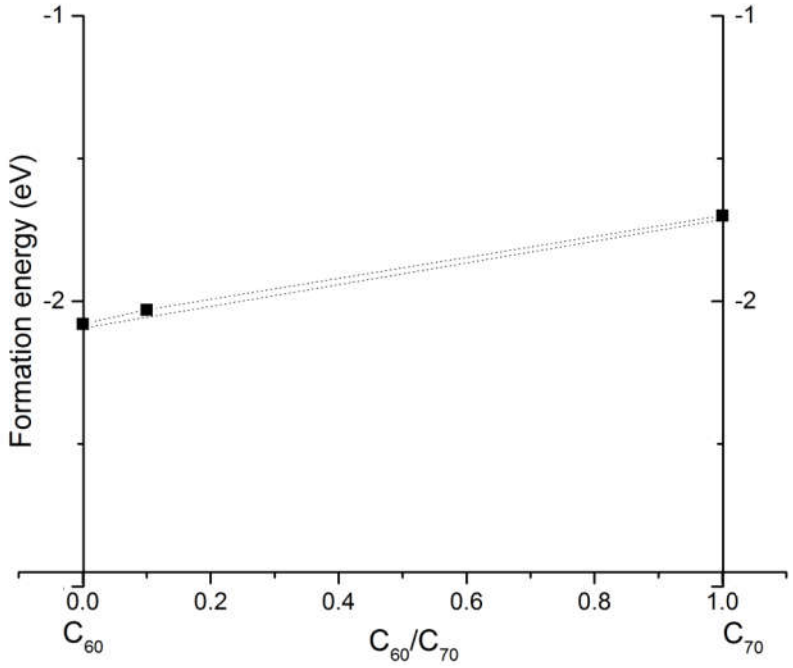

The electron transfer rate of C_{60}/C_{70} mixed system: the computed elecgron transfer rates that can be achieved with C_{60}/C_{70} mixed structure between C_{60}/C_{70} units are on the order of 10^{12} (highest 3.98×10^{12}/sec). Thus the electron transfer rate does not drop compared to pure C_{60} (4.9×10^{12}/sec) crystals (cf. 1.8×10^{13}/sec for pure C_{70})

Figure S12. Segregation mechanism calculation of C_{60} and C_{70} mixture and electron transfer rate calculation.

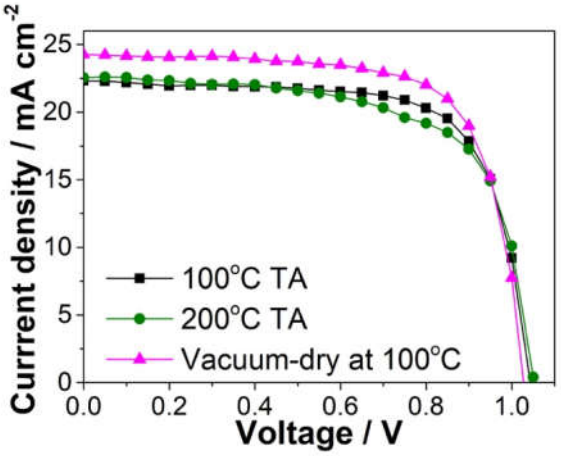

Figure S13. *J–V* curves of PSCs after 100 °C TA (green line), 200 °C TA (blue line), and 100 °C TA under light vacuum (purple line) on spin-coated mixed fullerene ETLs.

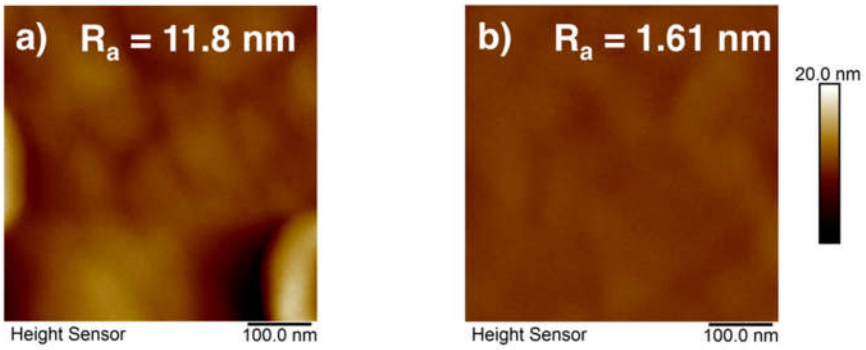

Figure S14. AFM images of a) 200 °C TA-treated spin-coated mixed fullerene film, and b) 100 °C TA-treated under light vacuum of spin-coated mixed fullerene film.

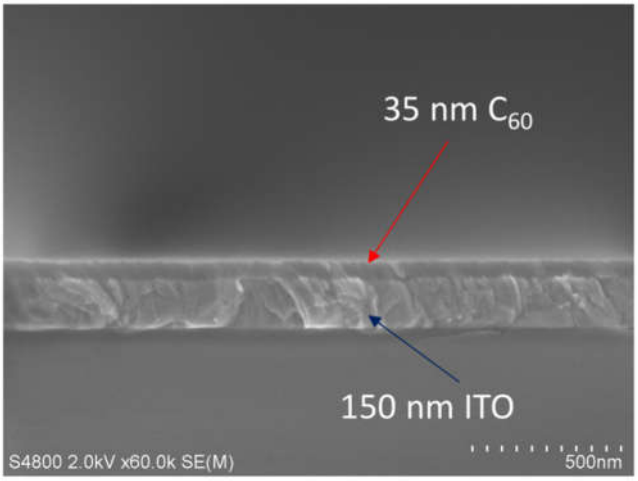

Figure S15. Cross sectional SEM of thermally deposited C_{60} on ITO substrate.

Table S2. Photovoltaic parameters of the normal-type PSCs using spin-coated C_{60}, C_{70} as the ETLs with vacuum-dry treatment under one sun (AM 1.5 G, 100 mW cm^{-2}).

Fullerene	J_{SC} [mA cm^{-2}]	V_{OC} [V]	FF	R_S [Ω cm^2]	R_{SH} [Ω cm^2]	PCE_{Best}	$PCE_{Average}$	Hysteresis Index
C_{60}	23.0	0.99	0.65	42	$1.7x10^4$	14.8%	14.6% ±0.7	0.03
Vacuum-dry C_{60}	24.1	0.99	0.67	37	$1.0x10^4$	16.0%	15.7% ±0.5	0.03
C_{70}	19.5	0.97	0.62	36	$6.8x10^4$	11.7%	11.4% ±0.6	0.07
Vacuum-dry C_{70}	21.7	0.98	0.60	38	$1.2x10^4$	12.1%	11.9% ±0.4	0.05

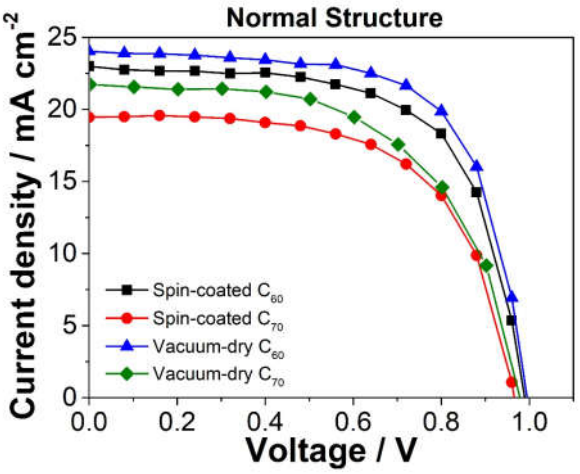

Figure S16. *J–V* curves of the normal-type PSCs using spin-coated C_{60} (black square), spin-coated C_{70} (red circle), vacuum-dry C_{60} (blue triangle), and vacuum-dry C_{70} (green diamond).

SUPPORTING REFERENCES

S1) Frisch, M. J.; Trucks, G. W.; Schlegel, H. B.; Scuseria, G. E.; Robb, M. A.; Cheeseman, J. R.; Scalmani, G.; Barone, V.; Mennucci, B.; Petersson, G. A.; Nakatsuji, H.; Caricato, M.; Li, X.; Hratchian, H. P.; Izmaylov, A. F.; Bloino, J.; Zheng, G.; Sonnenberg, J. L.; Hada, M.; Ehara, M.; Toyota, K.; Fukuda, R.; Hasegawa, J.; Ishida, M.; Nakajima, T.; Honda, Y.; Kitao, O.; Nakai, H.; Vreven, T.; Montgomery Jr., J. A.; Peralta, J. E.; Ogliaro, F.; Bearpark, M.; Heyd, J. J.; Brothers, E.; Kudin, K. N.; Staroverov, V. N.; Kobayashi, R.; Normand, J.; Raghavachari, K.; Rendell, A.; Burant, J. C.; Iyengar, S. S.; Tomasi, J.; Cossi, M.; Rega, N.; Millam, J. M.; Klene, M.; Knox, J. E.; Cross, J. B.; Bakken, V.; Adamo, C.; Jaramillo, J.; Gomperts, R.; Stratmann, R. E.; Yazyev, O.; Austin, A. J.; Cammi, R.; Pomelli, C.; Ochterski, J. W.; Martin, R. L.; Morokuma, K.; Zakrzewski, V. G.; Voth, G. A.; Salvador, P.; Dannenberg, J. J.; Dapprich, S.; Daniels, A. D.; Farkas, Ö.; Foresman, J. B.; Ortiz, J. V; Cioslowski, J.; Fox, D. J. Gaussian 09, Revision D.01. *Gaussian Inc.* **2009**, Wallingford CT.

S2) Becke, A. D. Density-functional thermochemistry. III. the role of exact exchange *J. Chem. Phys.* **1993**, *98*, 5648–5652.

S3) Perdew, J. P.; Burke, K.; Ernzerhof, M. Generalized gradient approximation made simple *Phys. Rev. Lett.* **1996**, *77*, 3865–3868.

S4) Aradi, B.; Hourahine, B.; Frauenheim, T. DFTB+, a sparse matrix-based implementation of the DFTB method *J. Phys. Chem. A* **2007**, *111*, 5678–5684.

S5) Lu, X.; Gaus, M.; Elstner, M.; Cui, Q. Parametrization of DFTB3/3OB for magnesium and zinc for chemical and biological applications *J. Phys. Chem. B* **2015**, *119*, 1062–1082.

S6) Kubillus, M.; Kubař, T.; Gaus, M.; Řezáč, J.; Elstner, M. Parameterization of the DFTB3 method for Br, Ca, Cl, F, I, K, and Na in organic and biological systems *J. Chem. Theory Comput.* **2015**, *11*, 332–342.

S7) Grimme, S. Semiempirical GGA-type density functional constructed with a long-range dispersion correction *J. Comput. Chem.* **2006**, *27*, 1787–1799.